A NEW CHANGE DETECTION TECHNIQUE APPLIED TO COSMO-SKYMED STRIPMAP HIMAGE DATA

A. Losurdo[(1)], C. Marzo[(2)], A. Guariglia [(1)]

[(1)]GEOCART S.p.A., Viale del Basento 120, 85100 Potenza, Italy, Email: {a.losurdo/a.guariglia}@geocart.net
[(2)] Agenzia Spaziale Italiana (ASI), C.da Terlecchia, 75100 Matera, Italy, Email: c.marzo@asi.it

ABSTRACT

Change Detection techniques in SAR images is very relevant for the locationing and the monitoring of interesting land changes. At present, it is a very important topic due to the high repetitiveness and of the new SAR satellite instruments (e.g. COSMO-SkyMed and Sentinel-1).
Geocart S.p.A. has reached important results about SAR change detection techniques within a technological project designed and implemented for the Italian Space Agency. The project's title is "Integrated Monitoring System: application to the GAS pipeline". The aim of the project is the development of a new remote sensing service integrating aerial and satellite data for GAS pipeline monitoring. An important Work-Package of the project aims to develop algorithms regarding the change detection to be applied on COSMO-SkyMed Stripmap Himage data in order to identify heavy lorries on pipelines.
Particularly, the paper presents a new change detection technique based on a probabilistic approach and the corresponding applicative results.

1. TEST SITE AND DATA SET

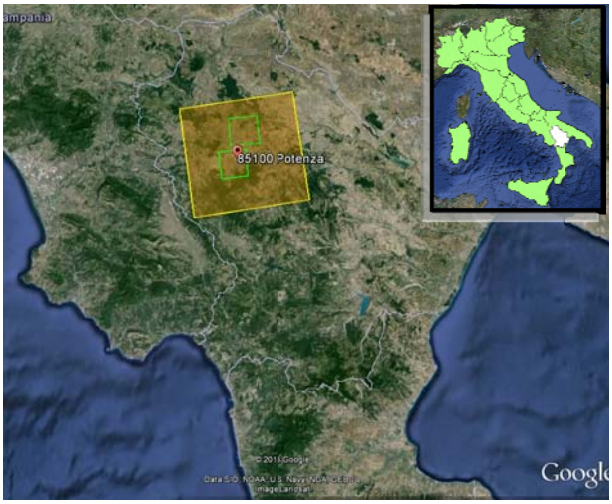

Figure 1. In orange Stripmap ascending "Potenza" scene and in green Spotlight ascending scenes in Google Earth Image. Basilicata Region (white colour) and Italy (green colour) indicated in the top-right square.

Some test sites in the Basilicata region (Southern Italy) have been chosen for the project. The test sites are localized in extra-urban area.
Test Site n.1. It is a little farm nearby a large plot of land aimed at arable and grazing land (Fig. 2-3-4).
Test Site n.2. It consists in a new-built cottage with wild land and building material around (Fig. 5-6-7). Different types of vehicles, with diverse position and orientation were placed on the test sites in order to simulate the presence of heavy lorries.
The used vehicles are a tractor of middle size (80 horsepower category) (Fig. 3-4) and a mini excavator (30 quintals category) (Fig. 6-7).
The test plan was implemented, step by step, according to the results achieved each time.

Figure 2. Test site n.1. Little farm area. The red star indicates the tractor's position on 19 February 2014, The yellow star indicates the position on 17 September 2014.

Figure 3. Tractor situated on 19 February 2014, west-east direction, on test site n.1.

Figure 4. Tractor situated on 17 September 2014, east-west direction, on test site n.1

The COSMO-SkyMed dataset used during the tests initially consist of 94 Stripmap data (25 descending and 69 ascending) covering Potenza Area. They were acquired for a previous work funded by the Italian Space Agency (ASI) under "COSMO-SyMed Announcement of Opportunity" (ID 1380, ASI Contract N. I/052/09/0).
In addition were acquired especially for the project three groups of COSMO-SkyMed data.
The first group includes Stripmap Himage data of the Map Italy program as detailed in Tab. 1.

Table 1. First COSMO-SkyMed Stripmap dataset

Satellite	Data	Geometria SAR
S4	2014-01-02 (Archivio)	Right Ascending
S4	2014-01-18 (Archivio)	Right Ascending
S4	2014 - 02 - 03	Right Ascending
S4	2014 - 02 - 19	Right Ascending
S4	2014 - 03 - 23*	Right Ascending
S4	2014 - 04 - 08	Right Ascending
S4	2014 - 07 - 29	Right Ascending

** radiometric degraded*

The application of the developed change detection algorithm, on first dataset, carries out maps of temporal changes.
During the first analysis, pixels corresponding to the position of the vehicles were not identified in the change detection maps. It happened because the method was incorrect.
For this reason the test sites and vehicles used for the second COSMO-SkyMed dataset were chosen with specific features:

1. To prearrange the scene with vehicle in a central position of an homogeneous area of minimum area equal to 60m*60m;
2. To direct vehicles with a favourable orientation for the geometrical acquisition of satellite data.

Figure 5. Test site n. 2. A new built cottage. The red star indicates the tractor's position on 19 February 2014 and on 08 April 2014 (first COSMO-SkyMed dataset). The yellow star indicates the tractor's position on 21-24 November 2014 (third COSMO-SkyMed dataset).

Figure 6. Mini Excavator located on 19 February and 08 April 2014

Figure 7. Mini Excavator situated on 21 and 24 November 2014

Table 2. Second COSMO-SkyMed Stripmap dataset

Satellite	Data	SAR Geometry
S1	2014-08-24	Right Ascending
S2	2014-09-01	Right Ascending
S1	2014-09-09	Right Ascending
S2	2014-09-17	Right Ascending
S1	2014-09-25	Right Ascending
S2	2014-10-03	Right Ascending

The third Stripmap and Spotlight datasets are aimed to compare the change detection performances using different COSMO-SkyMed data types in order to detect the same target, in the same position, on the same site.

Table 3. Third COSMO-SkyMed Stripmap dataset

Satellite	Data	SAR Geometry
S1	2014 - 11 - 12	Right Ascending (H4-16)
S3	2014 - 11 - 21	Right Ascending (H4-16)
S4	2014 - 11 - 19	Right Ascending (H4-20)
S1	2014 - 12 - 09	Right Ascending (H4-20)

Table 4. Third COSMO-SkyMed Spotlight dataset

Satellite	Data	SAR Geometry
S4	2014 - 11 - 24	Right Ascending (H4-16)
S2	2014 - 12 - 06	Right Ascending (H4-16)
S4	2014 - 12 - 10	Right Ascending (H4-16)
S3	2014 - 12 - 02	Right Ascending (H4-20)

2. CHANGE DETECTION TECHNIQUES

There are two different approaches to estimate changes with multi-temporal SAR satellite data. The former is based on a subjective visual interpretation and called visual change detection. The latter is founded on a probabilistic theory, as the developed new change detection technique.
Below are presented a classic visual change detection method with relative application case and the study done to achieve a new probabilistic change detection technique suitable for localizing vehicles of middle-large size, previously absent, on a rural background, the typical location of the gas pipeline network.

2.1. Visual Change Detection Techniques

Visual change detection techniques, for example the techniques called *"Interferometric Land Use"* or *"Multi-temporal Image"*, are characterized by the combination in different red/green/blue visualizations of the derived SAR products obtained by a pair of multi-temporal images of the same scene. The possible SAR products are amplitudes, coherences, differences and average amplitudes. Usually these change maps are produced for a qualitative assessment of damages in urban area after a natural disaster. In fact, the damaged buildings differently responds to the SAR's signal. It is evident analysing coherence images pre and post a destructive event. For this reason, the visual change detection techniques are not suitable to detect the changes in rural area.

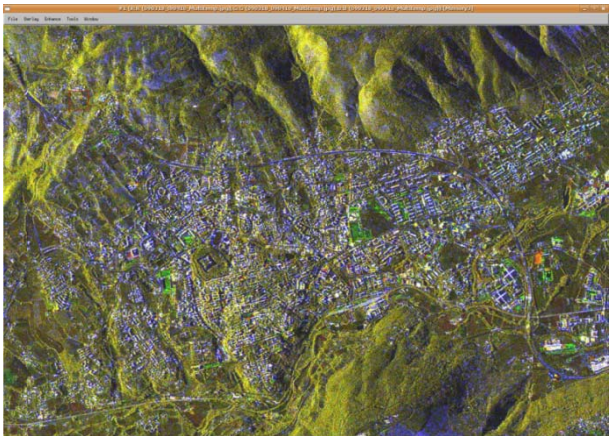

Figure 8. An example of a visual change detection map: Image of Aquila produced by a combination of derived products of COSMOSkyMed data pre and post the Earthquake on 06 April 2009 [1].

2.2. A New Change Detection Technique

The new change detection technique aims to evaluate a consistent and quantitative probability of a specific event and the related false alarm rate to predict a risk. The interesting event is the presence of a heavy lorry in rural areas where it previously was absent using multi-temporal Stripmap Himage data.
This event is very infrequent and at same time relevant for the gravity of a possible explosion which can be provoked by excavations in proximity of gas pipelines.
The rural area is characterized by large plots of land, buildings and man-made are very distant each other and very sparse.
We suppose valid for rural areas the speckle model developed for homogeneous areas by Chris Oliver and Shaun Quegan [2].
This SAR's speckle model is founded on the fact that a resolution cell contains numerous, infinite but numerable, scatters.
For large numbers of statistically identical scatters are valid the below rules:

1. The observed in-phase and in-quadrature components of the SAR signal are independent identically distributed Gaussian random variables with $\mu = 0$ ad variance equal to $\sigma/2$;
2. The measured phase will be evenly distributed in range $[-\pi; +\pi]$;
3. The observed intensity $I = A^2$ will be characterized by a negative exponential distribution with μ and standard deviation equal to σ, in case of image

with none multi-look applied, the probability distribution is:

$$P_I(I) = \frac{1}{\sigma}\exp\left(-\frac{I}{\sigma}\right) \quad \text{for } I \geq 0 \qquad (1)$$

These statistical distributions are fundamental in the SAR's signal processing. The target is completely described with σ parameter, and by Eq. 1 it is equal to Mean Intensity. When a pixel is characterized by many elementary scatters, the power observed is a measure of Radar Cross Section (RCS). If a pixel is part of a homogeneous area, σ can be estimate using the great quantity of pixels applying the mean operator.
In theory of probability, the Chi Square (χ^2) distribution describes the sum of the squares of some independent random variables characterized by a normal standard distribution. For this reason and for the previously assumptions SAR's intensity is described by a Chi Square distribution.

$$\chi^2 = \sum_{i=1}^{k} x_i^2 = x_1^2 + x_2^2 + x_3^2 \ldots\ldots\ldots\ldots\ldots + x_k^2 \qquad (2)$$

Where x_1, x_2, x_3 are independent random variables with Normal Distribution $\mathcal{N}(0,1)$ and where k is the degree of freedom.
If equation n.1 is valid, the SAR intensity, as the sum of two Gauss variables raised to the second power, arranges as a Chi Square variable.
The Chi Square probability is:

$$f_k(x) = \frac{1}{2^{\frac{k}{2}}\,\Gamma\left(\frac{k}{2}\right)}\, x^{\frac{k}{2}-1}\, e^{\frac{-x}{2}} \qquad (3)$$

K is the degree of freedom and equal to 2 for single look SAR data, characterized by the in-phase and in quadrature SAR's signal components.
On the other hand, Bruzzone and Bovolo [3] affirm that change detection in multi-temporal SAR images can be execute using Difference Operator, Ratio Operator and Logarithmic Ratio Operator.
Ratio Operator is preferable because it permits to equally estimate both areas with high intensity and areas with low intensity. Furthermore ratio operator allows to cancel common multiplicative noise.
The studies demonstrate that Ratio of SAR's intensities is modeled by the Fisher-Snedecor probability density function.
In the Eq. 4 the Fisher-Snedecor distribution of the ratio operator (X_R).

$$P(X_R) = \frac{1}{B\left(\frac{m}{2},\frac{n}{2}\right)}\,\frac{1}{X_R}\left(\frac{m^m\, n^n\, X_R^m}{(mX_R+n)^{m+n}}\right)^{1/2} \qquad (4)$$

The Fisher-Snedecor probability density function changes with the Equivalent Look Number (called *m* and *n*) of the utilized data.

The Equivalent Number of Look values:

$$< ENL > = L = \frac{\mu^2}{\sigma} \qquad (5)$$

If the target is characterized with Digital Number (DN) in change map equal to a value, called T, it is possible to calculate the false alarm rate defined as:

$$1 - P(X_R = T) \qquad (6)$$

The below Fig. 9 shows Fisher-Snedecor curves obtained with various ENL values. The red curve indicates the Fisher-Snedecor distribution by single-look data (m and n equal to 1) the green and blue curves the Fisher-Snedecor distributions by single look and multi-look SAR data (in particular case m equal to 1 and n equal to 3 and 5).
The false alarm rate decreases for high values, equally for multi-look SAR data.

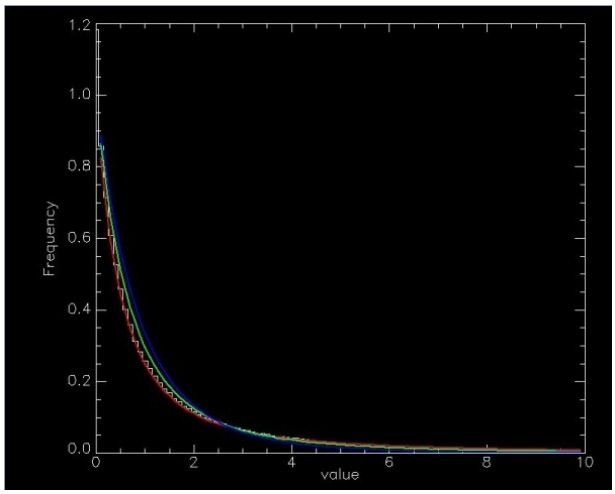

Figure 9. Fischer-Snedecor curves with ENL 1-1 (in red), ENL 1-3 (in green) and ENL 1-5 (in blu).

COSMO-SkyMed Stripmap Himage data are characterized by a swath extension of about 40 x 40 km^2 and a spatial resolution of 3x3 m^2 for single look. The change detection algorithm aims to detect targets as vehicles of middle-large size.
For these reasons a spatial multi-look results inapt because the interesting target has similar dimensions as the spatial resolution of the Stripmap data and the possibility of a temporal multi-look of SAR products was chosen.
In summary, the new change detection technique was design studying a probabilistic approach and following its innovative elements:

1. the opportunity to measure the probability of an event with the related False Alarm Rate and to predict a risk;

2. the use of a temporal multi-look in order to preserve the spatial information of the Stripmap data and at the same time to decrease the false alarm rate.

These properties are basic for an efficient and automatic monitoring service.

3. APPLICATION TO TEST SITES

Change Maps were obtained with the application of the Ratio Operator onto the multi-temporal Stripmap Himage pairs with/without the test target.
The targets were a tractor (80 horsepower category) in site test n. 1 and a mini excavator (30 quintals category) in site test n. 2 .

Location: test Site n.1; Target: the tractor situated on 19 February 2014 (Fig. 3).

Ratio Operator was applied to the interferometric Stripmap pairs: 19-03 February 2014 and 19 February 2014 - 08 April 2014.

Figure 10. Mean image obtained by 24 co-registered Stripmap data, the red star indicates the position of the tractor on 19 February 2014.

The search of those pixels in change detection images corresponding to the tractor is carried out in two attempts.
In the first attempt the mean image produced by co-registered data (within the pairs used in order to produce the change maps) was used to localize the area where the tractor is expected, in the second attempt tractor's pixel coordinates have been evaluated by geographic coordinates using a geocoding algorithm (by authors). Both specific area are overlapping each other.
Changed pixels were expected with Digital Number values very high. On the change map obtained with pair 19-3 February 2014 have been found in the specific area DNs equal to 290 and 1180, but they are not in the same pixel position on the co-registered change map by the pair 19 February 08 April 2014. Fig. 11 shows white pixels (correspondent of very high DN) not in the same location on the two change maps.

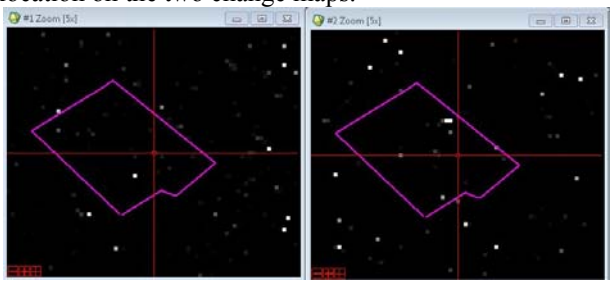

Figure 11. Change Maps with stretching in range [13, 800]

The deep study of the change maps induces to identify other pixels with lower Digital Number values (Tab. 5) compared to the ones identified previously, but they are in the same coordinates on both change maps (Fig. 12). They prove to be the true pixel relative to the tractor.
In this case the co-registered Stripmap data are interpolated for factor equal to 2 in range direction and 1 in azimuth direction in order to preserve the radar signal.

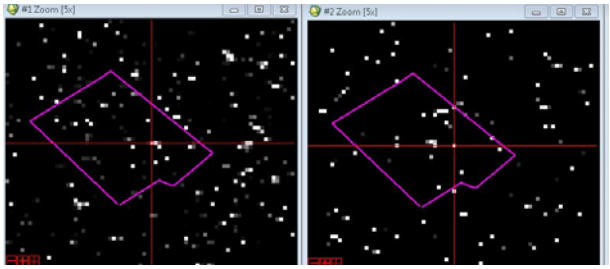

Figure 12. Change Maps with stretching in range [13, 80]. The cross centers the true change pixels identified.

Table 5. Change Detection results

Image 1	Image 2	DN_CD	Range	Azimuth	Prob_ theor	Prob_ exp
19/02	03/02	98.8	879	206	1.0	1.4
19/02	08/04	88.3	879	206	1.1	1.4

Location: test Site n.2; Target: mini excavator situated on 19 February 2014 and 08 April 2014 (Fig. 4).

Ratio Operator was applied to two groups of interferometric Stripmap pairs.
The two groups are composed of pairs characterized by a master data acquired when the excavator was in the site. So the data pairs of the first group are 19 - 03 February, 19 February -18 January, 19 February - 02 January and 19 February - 29 July 2014. Whereas the data pairs of the second group are characterized by the data acquired in 08 April 2014 as master data. These are 08April -03 February, 08 April- 02 January, 08 April - 18 January, 08 April -29 July 2014.
The search of those pixels corresponding to the mini-excavator in the eight change maps is carried out

similarly at the previous case, using the mean image produced by co-registered data to localize the specific area and using the algorithm of geocoding.

Table 6. Changed Digital Numbers

Image 1	Image 2	DN_ CD	Range	Azimuth	Prob theor	Prob_ exp
19/02	02/01	95	1073	1030	1.0	0.4
19/02	18/01	11	1074	1030	8.3	6.9
19/02	03/02	3.13	1074	1030	24	24
19/02	29/07	17	1074	1030	5.5	5.0
08/04	02/01	14.9	1073	1030	6.2	4.7
		13.7	1074	1031		
08/04	18/01	21.4	1074	1031	4.4	2.9
08/04	03/02	3.12	1075	1031	24	22
08/04	29/07	15.6	1074	1031	6.0	4.7
		50.9	1075	1031	1.9	1.0

The Tab. 6 reports for each change map the Changed Digital Number (called DN_CD) corresponding to the mini excavator with the related pixel coordinates, the theoretical and experimental false alarm probability.
The theoretical probability is computed by the Fisher-Snedecor Distribution (called *prob_theor* in Tab.6) and the experimental probability by the observed change detection values (*prob_exp* in Tab. 6).
The Changed Digital Numbers of the eight change maps show a local maximum value around the same pixel coordinates very unstable. The minimum are 3.12 and 3.13, the maximum is 95.
Interesting the fact that the minimum value for the two groups have been registered with the same *Image2* (Stripmap data acquired on 03 February 2014), this could be caused by a high noise in the data and/or a bad co-registration.
Kept out the Stripmap data acquired on 03 February 2014 the minimum changed DN became 11.

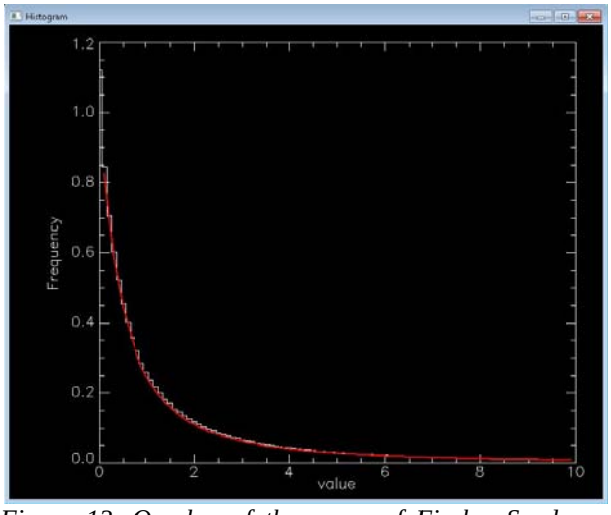

Figure 13. Overlay of the curve of Fischer-Snedecor with ENL 1-1 (in red) and experimental values of the Change map produced by the pair 08/04-03/02.

The second COSMO-SkyMed dataset (Tab. 2) is more numerous respect to the first and it was decisive to verify the applicability of the developed change detection algorithm.
Subsequently the description of the change results produced with the tractor in site test n. 1 as interesting target (Fig. 2-4).

Location: test site n.1; Target: the tractor situated on 17 September 2014 (Fig. 4).

The change maps were produced using the six Stripmap data of the second COSMO-SkyMed dataset (Tab. 2) and other three data acquired in 2011.
In this case the tractor is visible on the amplitude image produced by the Stripmap data with the test target (Fig. 14).

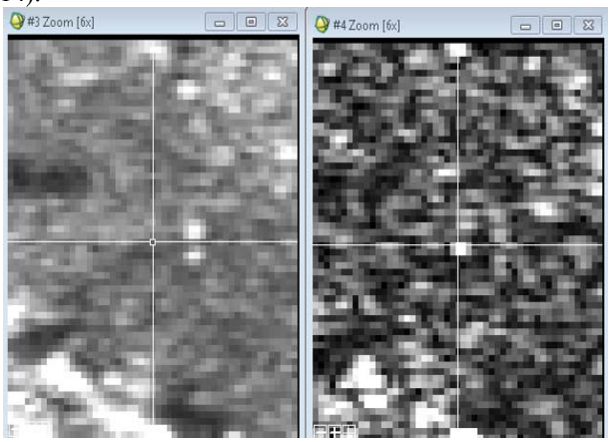

Figure 14. At left the mean image produced by 9 co-registered Stripmap data. At right the amplitude image by Stripmap data on 17/09/2014. They are centered on the tractor's position.

The results of the eight change maps show a local maximum value indicating a change in the range coordinates 1597-1598 and in the azimuth coordinates 602-603. The *DN_CD* values are very various, the minimum is 12.2 registered onto the change map by the pair 17 September 2014 - 13 September 2011 and the maximum is 149.2 in correspondence of the change map by pair 17 September - 24 August 2014. In the Tab. 7 all the features of the changed pixels.

Table 7. Changed Values resulting by single-look data

Img 1	Img 2	DN_ CD	Range	Azimu - th	Prob theor	Prob_ exp
17/09	09/09/14	20.1	1597	602	4.7	4.7
17/09	01/09/14	19.9	1597	602	4.7	4.9
17/09	24/08/14	149.2	1597	602	0.6	0.8
17/09	25/09/14	52.3	1597	603	1.8	2.0
17/09	03/10/14	24.8	1597	602	3.8	5.3
17/09	13/09/11	12.0	1598	603	7.7	8.1
17/09	16/08/11	75.7	1597	602	1.3	1.6
17/09	08/08/11	88.6	1598	603	1.1	1.4

Below the main features of the changed results.

1. The changed pixels corresponding to the position of the tractor are detected on all change maps (Tab. 7) obtained using the available multi-temporal pairs with/without the test target (advantage).
2. The Fisher-Snedecor probability function correctly models the experimental distribution of the changed DNs, in fact the probability of the false alarm (called *prob_theor* in tab. 7) well corresponds to the related experimental data (called *prob_exp* in Tab. 7) (advantage).
3. The Digital Number of the identified changed pixels and the relative false alarm probabilities are very various (disadvantage).

The change detection algorithm is optimized in order to overcome the aforementioned disadvantage using temporal multi-look products, tab. 8 reports the change detection results obtained with temporal multi-look data. The false alarm rates are very low.

Table 8. Change Detection results using time multi-look

Img_1	Img_2: mean image	DN_CD	Ran-ge	Azimu-th	Probtheor	Prob_exp
17/09	01/09/14	41.1	1598	602	0.21 (ENL=2)	0.25
	01/09/14					
	24/08/14					
17/09	17 data in Tab. 9	13.6	1597	602	0.3 (ENL=3.8)	0.11

Table 9. Stripmap data used for time multilook

Sat.	***date***	***Sat.***	***date***	***Sat.***	***date***
S2	20110723	S3	20110809	S4	20110828
S3	20110724	S4	20110812	S1	20110901
S1	20110731	S1	20110816	S2	20110909
S2	20110808	S2	20110824	S3	20110910
S4	20110913	S1	20140824	S1	20140909
S1	20110917	S2	20140917	S2	20140901

The third COSMO-SkyMed dataset is composed by Stripmap and Spotlight data.

Location: test Site n.2; Target: the mini-excavator situated on 21-24 November 2014 (Fig. 7)

The last test is aimed to compare the change detection performances using different COSMO-SkyMed data types in order to detect the same target, in the same position, on the same site. The change maps are obtained using four Stripmap Himage data and three Spotlight 2.

In tab. 10 the change detection results using single-look Stripmap and a temporal multi-look product obtained by the same single-look data. The theoretical and experimental probabilities of false alarm are equal to 2-3% using single Stripmap data (analyzing three multi-temporal pairs of single-look data), these values become 0.5 - 0.7 % using the mean image as a temporal multi-look product.

Table 10. Change Detection results with single-look and temporal multi-look Stripmap products

Img_1	Img_ 2	DN_CD	Range	Azimuth	Prob_theor	Probexp
21/11	12/11	52.1	1618	614	1.8	0.94
21/11	17/09	42.0	1619	615	2.3	1.4
21/11	03/10	33.2	1621	615	2.9	1.8
21/11	Mean Image by three data	24	1619	615	0.7 (ENL=1.9)	0.45
		18	1620	615		

Tab. 11 reports the DNs of the changed pixels on the Spotlight's change maps. The mini excavator causes high DNs on several close pixels in the two change maps. The false alarm probabilities measured with the Fisher-Snedecor Distribution (*prob_theor* in Tab.11) are very near to the correspondent values measured on the change maps (*prob_exp* in Tab.11).

Table 11. Change Detection results with single Spotlight data

Image 1	Image 2	DN_CD	Range	Azimuth	Prob_theor	Prob_exp
24/11	06/12	46	1580	614	2.1	0.8
		168	1580	615	0.6	0.06
		215	1579	614	0.4	0.03
		293	1578	614	0.3	0.01
24/11	10/12	43	1582	614	2.3	0.9
		142	1581	614	0.6	0.09
		41	1577	614	2.3	1.0
		43	1578	613	2.3	0.9
		44	1579	615	2.3	0.9
		112	1578	614	0.88	0.15
		679	1580	614	0.14	0.00
		711	1579	614	0.14	0.00

4. CONCLUSIONS AND OUTLOOKS

The main feature of the change detection technique is its quantitative method which allows a consistent measure of false alarm rate. Several tests are carried out in order to evaluate the algorithm's performance.

The main remarks of the study are:

- (General)
  The Fisher Snedecor distribution correctly models the experimental distribution of the change maps obtained by Stripmap and Spotligth data covering rural area (Fig. 13). In fact the theoretical probabilities are similar to the correspondent experimental probabilities (tab. 5-6-7-8-10-11).

- (referring to change maps by single-look Stripmap data)
  The target changed pixels are clearly identified by all multi-temporal pairs with/without the test target. The target change DNs are very unstable.
- (referring to change map by temporal multi-look Stripmap data).
  The false alarm probabilities of the interesting changes are within the range 0.11 % 0.7% , they are very low. The use of only three data to produce temporal multi-look products is sufficient to return a stability in change maps and to reduce the false alarm from a mean value of 5% to a mean value of 0.5 %.
- (what choose between change maps by temporal multi-look Stripmap and by single-look Spotlight data)
  The change detection algorithm with a time multi-look of three Stripmap data generates equivalent false alarm compared to the case of using single Spotlight data, with the precious advantage of a remote monitoring of a larger cover area.

5. ACKNOWLEDGMENT

This work is co-funded by the Italian Space Agency (ASI) under “Second Announcement for Small Medium Enterprise” (ASI contract N. I/010/12/0).

6. REFERENCES

1. http: //www.asi.it/ it/news/la_faglia_del_terremoto_individuata_grazie_ai_dati_di_cosmoskymed.

2. Chris Oliver and Shaun Quegan. Understanding Synthetic Aperture Radar Images © 2004 by SciTech Publishing, Inc. Raleigh, NC 27613 - 4° cap.

3. Bruzzone and Bovolo. Image Processing for Remote Sensing. by C.H. Chen – 5° cap.

4. Marzo, C., Losurdo, A., Guerriero & Colangelo, A. (2005). Esperienze di utilizzo di tecnologie SAR nel calcolo del Digital Elevation Model e nel monitoraggio di strutture edilizie interessate da deformazioni del territorio. *Bollettino AIC.* No. 123-124-125, pp. 525-533.

5. Kampes, B. M., Hanssen, R. F. & Perski, Z. (2003). Radar Interferometry with public domain tools. In Proc. *Third International Workshop on ERS SAR Interferometry, ‘FRINGE03’*. Frascati, Italy, 1-5 Dec. 2003.